HHS Public Access

Author manuscript

Kidney Int. Author manuscript; available in PMC 2023 September 01.

Published in final edited form as:

Kidney Int. 2022 September ; 102(3): 577–591. doi:10.1016/j.kint.2022.04.034.

Ttc21b deficiency attenuates autosomal dominant polycystic kidney disease in a kidney tubular- and maturation-dependent manner

Wei Wang[1], **Luciane M. Silva**[1], **Henry H. Wang**[1], **Matthew A. Kavanaugh**[1], **Tana S. Pottorf**[1], **Bailey A. Allard**[1], **Damon T. Jacobs**[1], **Rouchen Dong**[1], **Joseph T. Cornelius**[1], **Aakriti Chaturvedi**[1], **Katherine I. Swenson-Fields**[1], **Timothy A Fields**[2], **Michele T. Pritchard**[3], **Madhulika Sharma**[4], **Chad Slawson**[5], **Darren P. Wallace**[4], **James P. Calvet**[5], **Pamela V. Tran**[1]

[1]Dept. of Anatomy and Cell Biology, The Jared Grantham Kidney Institute, University of Kansas Medical Center, Kansas City, KS

[2]Dept. of Pathology and Laboratory Medicine, The Jared Grantham Kidney Institute, University of Kansas Medical Center, Kansas City, KS

[3]Pharmacology, Toxicology and Therapeutics, The Jared Grantham Kidney Institute, University of Kansas Medical Center, Kansas City, KS

[4]Dept. of Internal Medicine, The Jared Grantham Kidney Institute, University of Kansas Medical Center, Kansas City, KS

[5]Dept. of Biochemistry and Molecular Biology, The Jared Grantham Kidney Institute, University of Kansas Medical Center, Kansas City, KS

Abstract

Primary cilia are sensory organelles built and maintained by intraflagellar transport (IFT) multiprotein complexes. Deletion of several IFT-B genes attenuates polycystic kidney disease (PKD) severity in juvenile and adult autosomal dominant polycystic kidney disease (ADPKD) mouse models. However, deletion of an IFT-A adaptor, *Tulp3*, attenuates PKD severity in adult mice only. These studies indicate that dysfunction of specific cilia components has potential therapeutic value. To broaden our understanding of cilia dysfunction and its therapeutic potential, we investigate the role of global deletion of an IFT-A gene, *Ttc21b*, in juvenile and adult mouse

Correspondence should be addressed to: Pamela V. Tran, Department of Anatomy and Cell Biology and The Jared Grantham Kidney Institute, University of Kansas Medical Center, 3901 Rainbow Blvd., MS #3038, Kansas City, KS 66160, Tel: 913-945-7325; Fax: 913-588-2710, ptran@kumc.edu.

Disclosure Statement

The authors declare no interests to disclose.

Supplementary Material

Supplementary File (PDF)

Supplementary Methods

Supplementary References

Supplementary information is available on Kidney International's website.

models of ADPKD. Both juvenile (postnatal day 21) and adult (six months of age) ADPKD mice exhibited kidney cysts, increased kidney weight/body weight ratios, lengthened kidney cilia, inflammation, and increased levels of the nutrient sensor, O-linked β-N-acetylglucosamine (O-GlcNAc). Deletion of *Ttc21b* in juvenile ADPKD mice reduced cortical collecting duct cystogenesis and kidney weight/body weight ratios, increased proximal tubular and glomerular dilations, but did not reduce cilia length, inflammation, nor O-GlcNAc levels. In contrast, *Ttc21b* deletion in adult ADPKD mice markedly attenuated kidney cystogenesis and reduced cilia length, inflammation, and O-GlcNAc levels. Thus, unlike IFT-B, the effect of *Ttc21b* deletion in mouse models of ADPKD is development-specific. Unlike an IFT-A adaptor, deleting *Ttc21b* in juvenile ADPKD mice is partially ameliorative. Thus, our studies suggest that different microenvironmental factors, found in distinct nephron segments and in developing versus mature stages, modify ciliary homeostasis and ADPKD pathobiology. Further, elevated levels of O-GlcNAc, which regulates cellular metabolism and ciliogenesis, may be a pathological feature of ADPKD.

Graphical Abstract

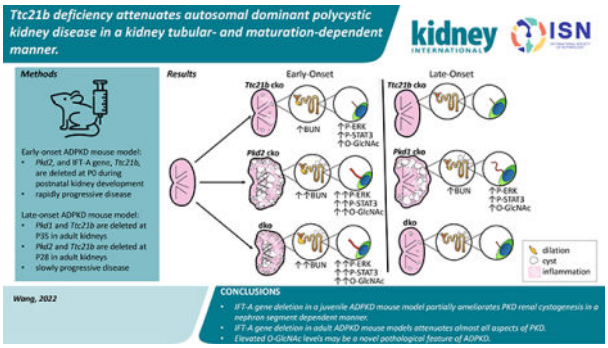

Keywords

Thm1 ; IFT139; ciliopathy; early-onset; late-onset; renal cystic disease

Introduction

Autosomal dominant polycystic kidney disease (ADPKD) is among the most common, fatal monogenetic diseases, affecting approximately 1:1000 individuals worldwide[1]. ADPKD is characterized by the growth of large fluid-filled kidney cysts, which cause injury and fibrosis and can lead to end-stage kidney disease by the 6th decade of life. Tolvaptan is the only available FDA-approved therapy but has variable effectiveness and aquaresis side effects[2, 3]. Thus, the need to discover additional underlying mechanisms and new therapeutic strategies continues.

Primary cilia are small antenna-like sensory organelles that play an important role in ADPKD via mechanisms that remain unclear. ADPKD is caused by mutations in *PKD1* or *PKD2*, which encode polycystin 1 (PC1) and polycystin 2 (PC2), respectively[4]. PC1 and PC2 form an ion-channel receptor complex that functions at the primary cilium. Although PC1 and PC2 localize to other subcellular compartments, analyses of human ADPKD

primary renal epithelial cells, of mouse models harboring human ADPKD mutations, and of an ethylnitrosourea (ENU)-induced *Pkd2* mouse mutation that causes ciliary exclusion of PC2, indicate that polycystin deficiency at the cilium is sufficient to cause ADPKD[5–7].

Primary cilia are synthesized and maintained via intraflagellar transport (IFT), which is the bidirectional transport of protein cargo along a microtubular axoneme. Two multiprotein complexes mediate IFT. The IFT-B complex interacts with the kinesin motor and mediates anterograde IFT, while the IFT-A complex together with cytoplasmic dynein mediates retrograde IFT. IFT-A proteins are also required for ciliary import of membrane and signaling molecules[8–10]. Additionally, an IFT-A adaptor, TULP3, binds to the IFT-A complex and brings in certain G-protein signaling molecules[9]. In mice, deletion of *Ift-A* or -*B* genes or of *Tulp3* perinatally or in the embryonic kidney results in renal cystic disease[11–13]. However, these mutants differ from ADPKD mouse models by manifesting smaller renal cysts and greater fibrosis relative to cyst size[14, 15]. Additionally, *Ift-A* and -*B* mutants differ in cilia phenotype often having shortened and absent cilia, respectively, and can have opposing signaling phenotypes, reflecting the differing functions of IFT-A and -B[12, 16–18]. Intriguingly, deletion of *Ift-B* genes, *Kif3a*, *Ift20* and *Ift88*, in juvenile or adult *Pkd1* or *Pkd2* conditional knock-out (cko) mice reduces PKD severity[19–21], while deletion of IFT-A adaptor, *Tulp3*, attenuates PKD in adult mice only[22, 23]. These studies indicate that a component of cilia dysfunction has potential therapeutic value.

The role of deletion of an IFT-A gene in ADPKD is unknown. *TTC21B* (*THM1*) is an orthologue of *Chlamydomonas* IFT-A gene, *IFT139*[16]. Causative or modifying mutations in *TTC21B* have been identified in patients with various renal diseases, including nephronophthisis, Bardet Biedl syndrome, Meckel syndrome, Jeune syndrome, familial focal segmental glomerulosclerosis, and renal agenesis[14, 24–26]. Characteristic of an IFT-A defect, deletion of *Ttc21b* impairs retrograde IFT, causing protein accumulation in bulb-like distal tips of shortened primary cilia[16]. *Ttc21b* loss also impairs cilia entry of membrane-associated proteins, delays and reduces ciliogenesis, and promotes serum-induced cilia loss[27]. In mice, *Ttc21b* deletion results in many of the clinical manifestations of ciliopathies[16, 28, 29]. Global deletion of *Ttc21b* in the perinatal period causes renal cystic disease affecting multiple nephron segments by 6 weeks of age[28]. In contrast, deletion of *Ttc21b* in adult mice does not cause a renal phenotype by 3 months of age[28], consistent with the developmental timeframe that determines whether loss of a cystogene causes rapid or slow-progressing renal cystic disease[30]. To expand on the potential therapeutic value of deleting specific cilia components in ADPKD, here we investigate the role of *Ttc21b* deficiency in juvenile and adult ADPKD mouse models.

Methods

Generation of mice

Pkd1$^{flox/flox}$, *Pkd2*$^{flox/flox}$ and *ROSA26-Cre* mice were obtained from the Jackson Laboratories (Stock numbers 010671, 017292 and 004847, respectively). *Ttc21b*$^{flox/flox}$ and *Ttc21b*$^{aln/+}$; *ROSA26Cre*$^{ERT+}$ colonies were generated as described[28]. *Pkd1* floxed alleles were introduced into these colonies to generate *Pkd1*$^{flox/flox}$;*Ttc21b*$^{flox/flox}$ or *Pkd1*$^{flox/+}$; *Ttc21b*$^{flox/flox}$; females and *Pkd1*$^{flox/flox}$; *Ttc21b*$^{aln/+}$, *ROSA26-Cre*$^{ERT/+}$ males.

These parental lines were mated to produce single and double knock-out (dko) mice (Supplementary Figure S1). *Pkd2*; *Ttc21b* colonies were generated in the same manner. To generate early-onset *Pkd2* models, nursing mothers were injected intraperitoneally with tamoxifen (8mg/40g; Sigma-Aldrich, T5648) at postnatal day 0 (P0) to induce gene deletion. Offspring were analyzed at P21. To generate late-onset *Pkd1* or *Pkd2* models, mice were injected intraperitoneally with tamoxifen (8mg/40g) at P35 or P28, respectively. Mice were analyzed at 6 months of age. All mouse lines were maintained on a pure C57BL6/J background (backcrossed ≥10 generations). All animal procedures were conducted in accordance with KUMC-IACUC and AAALAC rules and regulations.

Immunofluorescence

Paraffin-embedded tissue sections (10μm) were deparaffinized, rehydrated through an ethanol series, and subjected to antigen retrieval. Tissue sections were steamed for 15 minutes in Sodium Citrate Buffer (10 mM Sodium Citrate, 0.05% Tween 20, pH 6.0), returned to room temperature, rinsed 10 times in distilled water, washed 5 minutes in PBS, incubated for 5 minutes in 1% SDS in PBS based on a method by Brown et al., 1996[31], then washed 3 times in PBS. Immunofluorescence was performed as described[32], using primary antibodies alone or together with lectins (Supplementary Table S1) followed by secondary antibodies (Supplementary Table S2). Sections were mounted with DAPI Fluoromount-G (Electron Microscopy Sciences, 17984–24). Staining was imaged using a Nikon 80i microscope with a photometrics camera or a Nikon Eclipse TiE attached to an A1R-SHR confocal with an A1-DU4 detector and LU4 laser launch.

Immunohistochemistry

Immunohistochemistry was performed as described[33] using primary and secondary antibodies (Supplementary Tables S1, S2), and counterstained with haemotoxylin. Staining was imaged using a Zeiss A1 microscope with a Axiocam 105 color camera.

X-gal staining

Kidneys of P0, P2 and P7 mice harboring the *Ttc21b-lacZ* allele (Knockout Mouse Project Repository) were dissected, fixed for 5 min in 10% formalin, washed in lacZ wash buffer, then stained in X-gal solution (Teknova, X1220) at 37°C overnight as described[34]. Kidneys were fixed in 10% formalin at 4°C overnight, processed, then embedded. Sections were mounted in Permount or labelled with Dolichus Biflorus Agglutinin (DBA) or Lotus Tetragonolobus Lectin (LTL) then mounted in DAPI Fluoromount-G. Staining was imaged using brightfield or confocal microscopy as described[35].

Western blot

Western blots were performed as described[33]. Briefly, kidney pieces were homogenized in Passive Lysis Buffer (Promega, E1941) containing protease inhibitors (Thermofisher, A32965) using a BulletBlender Storm 24 (NextAdvance). To determine protein concentrations, BCA assays (ThermoFisher, 23227) were performed according to manufacturer's instructions. Protein lysates (50μg) were run on a gel, then transferred onto a Polyvinylidene Fluoride (PVDF) membrane (Sigma, P2938). Membranes were stained with

Ponceau S (Sigma, P3504), then incubated with primary and secondary antibodies (Tables S1 and S2). Western blots were quantified using ImageJ.

ADPKD and normal human kidney (NHK) sections

ADPKD (K386, K408, K423) and NHK (K357, K402, K419) sections were obtained from the PKD Biomarkers, Biomaterials, and Cellular Models Core in the Kansas PKD Center. The protocol for the use of discarded human tissues complied with federal regulations and was approved by the Institutional Review Board at KUMC[33].

Results

Perinatal deletion of *Ttc21b* in *Pkd2* cko mice reduces cortical collecting duct cystogenesis, but does not improve kidney function

To determine the effect of *Ttc21b* deficiency in a rapidly-progressing ADPKD mouse model, we deleted *Ttc21b* alone and together with *Pkd2* at P0 and examined the renal phenotypes at P21. At this early stage, *Ttc21b* cko mice on a C57BL6/J background showed renal cortical tubular dilations, reduced KW/BW ratios, and elevated blood urea nitrogen (BUN) levels (Figures 1A–1C). In contrast, *Pkd2* cko mice showed cysts in the cortex and medulla with increased KW/BW ratios and BUN levels. Additional deletion of *Ttc21b* in *Pkd2* cko mice decreased cystogenesis in the cortex (Figures 1D–1F), reduced KW/BW ratios, but did not affect BUN levels. *Ttc21b* cko renal cortical dilations were mostly proximal tubular (LTL+; Figure 1G), while *Pkd2* cko renal cortices further showed cysts originating from the loop of Henle (THP+) and the collecting duct (DBA+), which were the largest and most abundant. Deletion of *Ttc21b* in *Pkd2* cko mice increased proximal tubular dilations, did not affect THP+ cystogenesis, and decreased DBA+ cysts (Figures 1G–1I, Supplementary Figure S2). Glomerular dilations were also present in *Pkd2* cko kidneys and were increased in *Pkd2*; *Ttc21b* dko kidneys (Figures 1J, 1K). Thus, the effects of *Ttc21b* deletion on a *Pkd2* cko background appear nephron segment-specific.

Pkd2 deletion increases cilia lengths on renal epithelia

Since the effects of *Ttc21b* deletion in *Pkd2* cko mice occurred mostly in the renal cortex and cilia lengths vary with nephron segment[36, 37], we measured cilia lengths specifically in the inner cortex. In control kidneys, ciliary axonemes of LTL+ and DBA+ inner cortical tubular epithelial cells were 3.0μm- and 2.1μm in length, respectively (Figure 2). We also noted a qualitative difference with primary cilia of LTL+ cells being thin and wispy, while those of DBA+ cells were thicker and rod-like. In *Pkd2* cko cortices, cilia lengths of LTL+ and DBA+ cells were increased. In dko cortices, cilia lengths of LTL+ cells were further increased, but similar or slightly reduced in DBA+ cells, revealing tubular-specific effects.

Since TTC21B mediates both retrograde IFT[16] and ciliary import of membrane proteins[27], we examined contribution of these roles in the cilia phenotypes. In *Ttc21b* cko and dko kidneys, we observed accumulation of IFT81 in bulbous ciliary distal tips, reflecting impaired retrograde IFT (Figure 2C). In contrast, ciliary localization and staining intensity of ciliary membrane protein, ARL13B, appeared similar in DBA+ cortical renal epithelial cells across the mutant genotypes (Supplementary Figure S3). These data indicate that the

role of TTC21B in retrograde IFT has a stronger influence on the renal cilia phenotypes *in vivo*.

To determine whether differential expression of *Ttc21b* in proximal tubules versus cortical collecting ducts may account for the nephron-specific effects, X-gal staining on kidneys of mice harboring a *Ttc21b-lacZ* allele was performed. At P0 and P2, Ttc21b-lacZ expression was relatively ubiquitous in all tubules (Supplementary Figure S4). Thus, differences in cilia phenotypes in the proximal tubules and cortical collecting ducts might be attributed to differences in the microenvironments of these nephron segments.

Perinatal deletion of *Ttc21b* increases inflammation

To further evaluate the effect of *Ttc21b* deletion on disease severity, we examined proliferation as well as inflammation and fibrosis. Proliferation was slightly elevated in dko LTL+ renal tubules, increased in *Pkd2* cko and dko DBA+ non-cystic tubules, and further increased in *Pkd2* cko and dko DBA+ cysts (Figures 3A–3C, Supplementary Figure S5). Increased proliferation in dko LTL+ renal tubules supports a genetic interaction between *Pkd2* and *Ttc21b* that exacerbates the proximal tubular phenotype. Additionally, increased proliferation of *Pkd2*-deficient non-cystic tubules substantiates that proliferation is an early cellular event in ADPKD renal cystogenesis[38].

In ADPKD, inflammation and fibrosis result from cysts compressing surrounding parenchyma causing injury. Histology revealed increased inflammatory cells and interstitial space in *Pkd2* cko and dko kidneys (Figure 3D). Consistent with this, picrosirius red staining for collagen, and immunostaining for macrophages (F4/80) and myofibroblasts (αSMA), which contribute to pro-inflammatory and pro-fibrotic processes, were increased around *Ttc21b* cko glomeruli and tubular dilations, and further increased in *Pkd2* cko and dko kidneys (Figures 3E–3J). Additionally, inflammatory cytokines, *Il6*, *Tnfα*, *Tgfβ*, *Ccl2* and *Gli1*, were increased in all mutant renal extracts (Figures 3K–3O). Thus, deletion of *Ttc21b* alone causes inflammation, and its deletion on a *Pkd2* cko background causes similar or slightly increased ADPKD inflammation at P21.

We next examined ERK and STAT3 signaling pathways, which have proliferative and inflammatory roles in ADPKD[39–45]. P-ERK intensity and P-STAT3 staining were increased in dilated tubules of *Ttc21b* cko mice, and further increased in cyst-lining cells of *Pkd2* cko and dko mice (Supplementary Figures S6A–S6D). Western blot analyses showed increased ERK and STAT signaling in *Pkd2* cko renal extracts and even greater activation in dko renal extracts (Supplementary Figures S6E–S6G). Thus, *Ttc21b* loss alone increases ERK and STAT3 activation, and together with deletion of *Pkd2* causes even greater ERK and STAT3 signaling than loss of *Pkd2* alone.

Pkd2 deletion increases O-GlcNAc levels in the kidney

Altere cellular metabolism has emerged as another component of ADPKD pathobiology[46–49]. O-linked β-N-acetylglucosamine (O-GlcNAc) tunes cellular functions in response to the nutrient microenvironment and is a product of the hexosamine biosynthetic pathway, which is initiated by glucose and ATP[50]. O-GlcNAc levels regulate mitochondrial function[50, 51], and more recently, have been shown to regulate ciliary homeostasis[52, 53].

Since both mitochondrial function and ciliary homeostasis are altered in ADPKD[46, 54], we hypothesized that O-GlcNAc signaling is misregulated in PKD. To assess O-GlcNAc signaling, we examined levels of O-GlcNAc as well as of O-GlcNAc transferase (OGT) and O-GlcNAcase (OGA), which are the enzymes that transfer and remove the O-GlcNAc moiety on protein substrates, respectively. In *Pkd2* cko and dko kidneys, O-GlcNAc, OGT and OGA were increased in cyst-lining cells (Figures 4A–4D, Supplementary Figure S7). Western blot analyses also showed increased O-GlcNAc levels in *Pkd2* cko and dko renal extracts (Figures 4E, 4F). These data suggest that increased O-GlcNAc signaling may be a pathological feature of ADPKD.

Deletion of *Ttc21b* in adult *Pkd1* or *Pkd2* cko mice markedly attenuates PKD renal cystogenesis

We next examined the role of *Ttc21b* deficiency in slowly progressive *Pkd1* and *Pkd2* cko adult mouse models. At 6 months of age, *Ttc21b* cko mice showed normal kidney morphology and BUN levels (Supplementary Figures S8A–S8D). In *Pkd1* cko and *Pkd2* cko mice, renal cysts were mostly in the cortex, with the largest and most abundant cysts being DBA+, and fewer and smaller cysts being THP+ or LTL+ (Figures 5A and 5B). However, deletion of *Ttc21b* in *Pkd1* or *Pkd2* cko adult mice markedly attenuated cysts of all tubular origins. In *Pkd1* cko mice, KW/BW ratios and BUN levels were elevated, butt additional deletion of *Ttc21b* corrected these parameters (Figures 5C, 5D). In *Pkd2* cko mice, KW/BW ratios were similar to control and BUN levels showed a trend toward a slight elevation, reflecting the mild disease induced in adulthood. Deletion of *Ttc21b* in *Pkd2* cko mice slightly reduced KW/BW ratios, likely due to increased body weight caused by global deletion of *Ttc21b*[29], while BUN levels were not significantly altered (Figure 5E, 5F).

Deletion of *Ttc21b* in adult *Pkd1* or *Pkd2* cko mice reduces cilia lengths of cortical collecting duct renal epithelia

Cilia lengths of *Pkd1* cko and *Pkd2* cko DBA+ adult renal inner cortical epithelial cells were increased, and deletion of *Ttc21b* in either *Pkd1* or *Pkd2* cko mice reduced DBA+ renal epithelial cilia lengths (Figures 5G, 5H, 5J, 5K). Additionally, human ADPKD cortical sections showed longer renal epithelial cilia than normal human kidney (NHK) sections (Figures 5I, 5L), supporting that increased cilia lengths is a feature of the human disease[21].

Deletion of *Ttc21b* in adult *Pkd1* cko mice reduces proliferation, inflammation, and O-GlcNAc

To assess the extent of ADPKD attenuation by *Ttc21b* deletion, we examined proliferation and inflammation. *Pkd1* cko kidneys showed increased proliferation of cyst-lining cells, and increased macrophages (F4/80) and myofibroblasts (αSMA) surrounding cysts and glomeruli, which were all markedly reduced in dko kidneys (Figures 6A–D). Inflammatory cytokines were also elevated in *Pkd1* cko kidneys but reduced in dko kidneys (Figure 6E–6I). Similarly, ERK and STAT3 activation were increased in *Pkd1* cko kidneys but reduced in dko kidneys (Supplementary Figures S9A, S9B). Thus, deletion of *Ttc21b* in late-onset *Pkd1* cko mice attenuates proliferative and inflammatory pathways.

Finally, we examined O-GlcNAc signaling. O-GlcNAc, OGT and OGA were increased in cyst-lining epithelia of *Pkd1* cko cortex and medulla (Figure 6J, Supplementary Figure S10), but reduced and similar to control in dko kidneys. Western blot also showed increased O-GlcNAc levels in *Pkd1* cko renal extracts, but reduced O-GlcNAc in dko extracts (Figure 6K, 6L). These data suggest increased O-GlcNAc is a feature of slowly-progressive ADPKD. Further, *Ttc21b* deletion in adult ADPKD mice attenuates O-GlcNAc elevation.

Discussion

Our study expands on the therapeutic potential of deleting ciliary genes in ADPKD mouse models[19, 22, 23]. In contrast to IFT-B genes, but similar to IFT-A adaptor gene, *Tulp3*, deletion of IFT-A gene, *Ttc21b*, did not attenuate renal function in an early-onset ADPKD model, but markedly attenuated almost all aspects of ADPKD in late-onset models. Yet distinct from *Tulp3*[23], global deletion of *Ttc21b* in an early-onset model reduced cortical collecting duct cystogenesis and KW/BW ratios. However, the effects of *Ttc21b* deletion in early-onset ADPKD mice appeared nephron-specific, with no effect on loop of Henle-derived cysts and worsening of proximal tubular and glomerular dilations. This may reflect varying microenvironments between nephron segments. The differential effects of *Tulp3* or *Ttc21b* deletion in early- versus late-onset ADPKD mouse models may also suggest differences in developing versus mature renal microenvironments. These data highlight the importance of renal context and examining molecules and pathways by cell type in the kidney.

The attenuation of ADPKD in adult *Pkd*;*cilia* dko mice indicates cilia genes are epistatic to *Pkd1* and *Pkd2*. Cilia genes may act upstream of *Pkd1* and *Pkd2* by providing the structural environment - both the compartment and neighboring proteins - for PC1 and PC2. As a compartment, the length of the cilium is interconnected with cilia function, and this interconnection is lost in ADPKD. In normal cells, increased cilia lengths enhance cilia sensory function, and in a cilium-dependent manner, fluid flow increases intracellular Ca^{2+} and reduces cilia lengths[55–60]. Studies indicate cilia lengths are aberrantly increased in ADPKD renal tissue[21, 38, 61], yet cultured *Pkd1*- or *Pkd2*-mutant renal epithelial cells have an abrogated cilia response to fluid flow, such that neither an increase in intracellular Ca^{2+} nor a decrease in cilia lengths are induced[57, 58]. We hypothesize that correcting cilia lengths in ADPKD, such as by deletion of *Ttc21b*, may offset the disconnect between cilia length and function. Cilium length itself may tune signaling pathways by affecting ability of signaling molecules to interact optimally. For instance, the position of an ion channel along the length of the cilium affects its activity[62]. Another possible mechanism is that in the absence of a particular IFT gene, certain signaling molecules may not reach the cilium, keeping proliferative and inflammatory signaling pathways from being aberrantly activated when PC1 or PC2 is missing. Since deletion of IFT-B, IFT-A or IFT-adaptor genes in adult ADPKD mouse models all attenuate PKD, these proposed mechanisms may unify and act downstream of the unique functions of individual IFT proteins.

In contrast, the different effects of deletion of IFT-B, IFT-A or IFT-A adaptor genes in juvenile ADPKD mouse models highlight the distinct roles of individual IFT proteins, including between TTC21B and TULP3. The IFT-A complex is comprised of 3 core

subunits and 3 peripheral subunits. TTC21B is a peripheral subunit thought to be situated most distally from the core proteins, while TULP3 binds to a core subunit furthest away from TTC21B[63]. As an IFT-A protein, TTC21B mediates retrograde IFT[16]. As an IFT-A adaptor, TULP3 does not mediate retrograde IFT, but shuttles certain G-protein coupled receptors into the cilium[9]. In cultured retinal pigment epithelial (RPE) cells and mouse embryonic fibroblasts, TULP3 and TTC21B, respectively, have shown to mediate ciliary import of membrane protein, ARL13B[27, 64]. However, while ARL13B was reduced in cilia of *Tulp3* mutant kidneys[22, 23], ciliary ARL13B was not markedly altered in *Ttc21b* cko and *Pkd2*;*Ttc21b* dko juvenile kidneys. Additionally, ciliary PC2 was reduced in *Tulp3* mutant kidneys[23]. In contrast, our data indicate that in *Ttc21b* knock-down inner mouse collecting duct (IMCD) cells, PC2 accumulates in bulbous ciliary distal tips (data not shown). Thus, differences in IFT function, IFT binding partners and cargoes could account for why deletion of *Ttc21b*, but not of *Tulp3*, partially attenuates early-onset ADPKD disease.

We also observed that inflammation was differentially regulated between juvenile and adult ADPKD mouse models. The inability of *Ttc21b* deficiency to attenuate inflammation in juvenile *Pkd2* cko mice likely prevented the amelioration of kidney function. In contrast, IFT-B (*Ift20*, *Kif3a*) gene deletion in juvenile ADPKD models improved kidney function[19]. There are inflammatory pathways that are cilium-dependent. Loss of cilia via *Kif3a* deletion in a juvenile ADPKD mouse model attenuated *Ccl2* expression and macrophage recruitment[20]. Outside of the kidney, in chondrocytes, IL-1 signaling elongates primary cilia, and in *IFT88*-mutant cells lacking cilia, IL-1 signaling was markedly reduced[65]. Additionally, in cartilage, mechanical loading is anti-inflammatory and suppressed IL-1 signaling by activating histone deacetylase 6 (HDAC6), which reduced tubulin acetylation and shortened cilia[66]. Whether mechano-regulation of inflammatory pathways extends to primary cilia in the kidney and the mechanisms by which IFT-A proteins regulate inflammation remain to be explored.

Finally, our data suggest elevated O-GlcNAcylation may be a feature of ADPKD. Increased O-GlcNAcylation is a pathologic feature of diabetic nephropathy[67, 68], and in rodent models, has shown to promote various aspects of chronic kidney disease[69, 70] as well as renal fibrosis[71]. In contrast, in a mouse model of contrast-induced acute kidney disease, an acute increase in O-GlcNAcylation was protective[72], emphasizing important differences between chronic and acute increases in O-GlcNAcylation. While acute changes are adaptive and necessary to maintain cellular health and metabolism, chronic changes are likely to contribute to pathology[73]. Perturbation of O-GlcNAcylation also affects cilia lengths[52, 53], and the ciliary structural defects caused by *Ogt* deletion in mice suggest impaired centriole formation and IFT[53]. Elucidating the mechanisms by which O-GlcNAc is upregulated in ADPKD and alters cellular metabolism and ciliogenesis could reveal novel mechanisms and therapeutic targets.

The limitations of our study include the lack of an early-onset *Pkd1* model to compare with the late-onset *Pkd1* model. The increased severity of *Pkd1*-mediated disease[74] may indicate functional differences between PC1 and PC2. However, since IFT-B gene deletion attenuates early-onset PKD disease in both *Pkd1* and *Pkd2* cko juvenile mice[19], *Ttc21b*

deficiency might partially attenuate *Pkd1* early-onset disease as it did for *Pkd2*. Additionally, our extensive efforts to examine absolute levels of *Ttc21b* in proximal tubules versus in collecting ducts were not successful, thus it is possible that differential *Ttc21b* expression levels could have also contributed to the dko phenotypes. However, Ttc21b-lacZ expression in the kidney appeared relatively ubiquitous, the *Rosa26-Cre*^{ERT} is globally expressed, and previously we observed cysts originating from proximal tubules, loop of Henle and collecting ducts in P42 early-onset *Ttc21b* cko; *Rosa26-Cre*^{ERT} mice on a mixed strain background[28], indicating tamoxifen reached these tubules. Further, while this study focused on the pathology of *Pkd*;*Ttc21b* dko kidneys, identifying the proteins resident in cilia of specific nephron segments is important to elucidating underlying mechanisms.

In summary, our data suggest cilia may have differential roles between nephron segments and between developing and mature kidneys. Our findings also reveal that O-GlcNAcylation is increased in ADPKD. We propose that as a regulator of ciliary homeostasis and cellular metabolism, elevated O-GlcNAc levels may underlie ADPKD pathological processes.

Supplementary Material

Refer to Web version on PubMed Central for supplementary material.

Acknowledgements

We thank members of the KUMC Department of Anatomy and Cell Biology and the Jared Grantham Kidney Institute for helpful discussions. We thank Jing Huang of the KUMC Histology Core, which is supported by NIH U54HD090216 and NIH P30GM122731. We also thank Pat St. John and Larysa Stroganova of the KUMC Electron Microscopy Research Laboratory, which is supported by NIH P20GM104936. This work was also supported by a K-INBRE Summer Student Award to JTC (K-INBRE P20GM103418), the PKD Biomaterials and Biomarkers Repository Core in the Kansas PKD Research and Translational Core Center (NIH P30DK106912 to JPC), R01DK108433 to MS, and R01DK103033 to PVT.

References

1. Lanktree MB, Haghighi A, Guiard E, et al. Prevalence Estimates of Polycystic Kidney and Liver Disease by Population Sequencing. J Am Soc Nephrol 2018; 29: 2593–2600. [PubMed: 30135240]
2. Torres VE, Chapman AB, Devuyst O, et al. Tolvaptan in patients with autosomal dominant polycystic kidney disease. N Engl J Med 2012; 367: 2407–2418. [PubMed: 23121377]
3. Blair HA. Tolvaptan: A Review in Autosomal Dominant Polycystic Kidney Disease. Drugs 2019.
4. Torres VE, Harris PC. Mechanisms of Disease: autosomal dominant and recessive polycystic kidney diseases. Nat Clin Pract Nephrol 2006; 2: 40–55; quiz 55. [PubMed: 16932388]
5. Freedman BS, Lam AQ, Sundsbak JL, et al. Reduced ciliary polycystin-2 in induced pluripotent stem cells from polycystic kidney disease patients with PKD1 mutations. J Am Soc Nephrol 2013; 24: 1571–1586. [PubMed: 24009235]
6. Cai Y, Fedeles SV, Dong K, et al. Altered trafficking and stability of polycystins underlie polycystic kidney disease. J Clin Invest 2014; 124: 5129–5144. [PubMed: 25365220]
7. Walker RV, Keynton JL, Grimes DT, et al. Ciliary exclusion of Polycystin-2 promotes kidney cystogenesis in an autosomal dominant polycystic kidney disease model. Nature communications 2019; 10: 4072.
8. Fu W, Wang L, Kim S, et al. Role for the IFT-A Complex in Selective Transport to the Primary Cilium. Cell reports 2016; 17: 1505–1517. [PubMed: 27806291]
9. Mukhopadhyay S, Wen X, Chih B, et al. TULP3 bridges the IFT-A complex and membrane phosphoinositides to promote trafficking of G protein-coupled receptors into primary cilia. Genes Dev 2010; 24: 2180–2193. [PubMed: 20889716]

10. Liem KF Jr., Ashe A, He M, et al. The IFT-A complex regulates Shh signaling through cilia structure and membrane protein trafficking. J Cell Biol 2012; 197: 789–800. [PubMed: 22689656]
11. Yoder BK, Tousson A, Millican L, et al. Polaris, a protein disrupted in orpk mutant mice, is required for assembly of renal cilium. American journal of physiology Renal physiology 2002; 282: F541–552. [PubMed: 11832437]
12. Jonassen JA, SanAgustin J, Baker SP, et al. Disruption of IFT complex A causes cystic kidneys without mitotic spindle misorientation. J Am Soc Nephrol 2012; 23: 641–651. [PubMed: 22282595]
13. Lin F, Hiesberger T, Cordes K, et al. Kidney-specific inactivation of the KIF3A subunit of kinesin-II inhibits renal ciliogenesis and produces polycystic kidney disease. Proc Natl Acad Sci U S A 2003; 100: 5286–5291. [PubMed: 12672950]
14. Davis EE, Zhang Q, Liu Q, et al. TTC21B contributes both causal and modifying alleles across the ciliopathy spectrum. Nat Genet 2011; 43: 189–196. [PubMed: 21258341]
15. Srivastava S, Molinari E, Raman S, et al. Many Genes-One Disease? Genetics of Nephronophthisis (NPHP) and NPHP-Associated Disorders. Front Pediatr 2017; 5: 287. [PubMed: 29379777]
16. Tran PV, Haycraft CJ, Besschetnova TY, et al. THM1 negatively modulates mouse sonic hedgehog signal transduction and affects retrograde intraflagellar transport in cilia. Nat Genet 2008; 40: 403–410. [PubMed: 18327258]
17. Qin J, Lin Y, Norman RX, et al. Intraflagellar transport protein 122 antagonizes Sonic Hedgehog signaling and controls ciliary localization of pathway components. Proceedings of the National Academy of Sciences of the United States of America 2011; 108: 1456–1461. [PubMed: 21209331]
18. Eggenschwiler JT, Anderson KV. Cilia and developmental signaling. Annual review of cell and developmental biology 2007; 23: 345–373.
19. Ma M, Tian X, Igarashi P, et al. Loss of cilia suppresses cyst growth in genetic models of autosomal dominant polycystic kidney disease. Nat Genet 2013; 45: 1004–1012. [PubMed: 23892607]
20. Viau A, Bienaime F, Lukas K, et al. Cilia-localized LKB1 regulates chemokine signaling, macrophage recruitment, and tissue homeostasis in the kidney. EMBO J 2018; 37.
21. Shao L, El-Jouni W, Kong F, et al. Genetic reduction of cilium-length by targeting intraflagellar transport 88 protein impedes kidney and liver cysts formation in mouse models of autosomal polycystic kidney disease. Kidney Int 2020.
22. Legue E, Liem KF Jr. Tulp3 Is a Ciliary Trafficking Gene that Regulates Polycystic Kidney Disease. Curr Biol 2019; 29: 803–812 e805. [PubMed: 30799240]
23. Hwang SH, Somatilaka BN, Badgandi H, et al. Tulp3 Regulates Renal Cystogenesis by Trafficking of Cystoproteins to Cilia. Curr Biol 2019; 29: 790–802 e795. [PubMed: 30799239]
24. Huynh Cong E, Bizet AA, Boyer O, et al. A homozygous missense mutation in the ciliary gene TTC21B causes familial FSGS. J Am Soc Nephrol 2014; 25: 2435–2443. [PubMed: 24876116]
25. Shaheen R, Sebai MA, Patel N, et al. The genetic landscape of familial congenital hydrocephalus. Ann Neurol 2017; 81: 890–897. [PubMed: 28556411]
26. Shamseldin HE, Shaheen R, Ewida N, et al. The morbid genome of ciliopathies: an update. Genet Med 2020; 22: 1051–1060. [PubMed: 32055034]
27. Wang W, Allard BA, Pottorf TS, et al. Genetic interaction of mammalian IFT-A paralogs regulates cilia disassembly, ciliary entry of membrane protein, Hedgehog signaling, and embryogenesis. FASEB J 2020.
28. Tran PV, Talbott GC, Turbe-Doan A, et al. Downregulating hedgehog signaling reduces renal cystogenic potential of mouse models. J Am Soc Nephrol 2014; 25: 2201–2212. [PubMed: 24700869]
29. Jacobs DT, Silva LM, Allard BA, et al. Dysfunction of intraflagellar transport-A causes hyperphagia-induced obesity and metabolic syndrome. Dis Model Mech 2016; 9: 789–798. [PubMed: 27482817]
30. Piontek K, Menezes LF, Garcia-Gonzalez MA, et al. A critical developmental switch defines the kinetics of kidney cyst formation after loss of Pkd1. Nat Med 2007; 13: 1490–1495. [PubMed: 17965720]

31. Brown D, Lydon J, McLaughlin M, et al. Antigen retrieval in cryostat tissue sections and cultured cells by treatment with sodium dodecyl sulfate (SDS). Histochem Cell Biol 1996; 105: 261–267. [PubMed: 9072183]
32. Silva LM, Wang W, Allard BA, et al. Analysis of primary cilia in renal tissue and cells. Methods Cell Biol 2019; 153: 205–229. [PubMed: 31395380]
33. Silva LM, Jacobs DT, Allard BA, et al. Inhibition of Hedgehog signaling suppresses proliferation and microcyst formation of human Autosomal Dominant Polycystic Kidney Disease cells. Scientific reports 2018; 8: 4985. [PubMed: 29563577]
34. Stottmann RW, Tran PV, Turbe-Doan A, et al. Ttc21b is required to restrict sonic hedgehog activity in the developing mouse forebrain. Dev Biol 2009; 335: 166–178. [PubMed: 19732765]
35. Levitsky KL, Toledo-Aral JJ, Lopez-Barneo J, et al. Direct confocal acquisition of fluorescence from X-gal staining on thick tissue sections. Scientific reports 2013; 3: 2937. [PubMed: 24121824]
36. Pazour GJ, Dickert BL, Vucica Y, et al. Chlamydomonas IFT88 and its mouse homologue, polycystic kidney disease gene tg737, are required for assembly of cilia and flagella. J Cell Biol 2000; 151: 709–718. [PubMed: 11062270]
37. Saraga-Babic M, Vukojevic K, Bocina I, et al. Ciliogenesis in normal human kidney development and post-natal life. Pediatr Nephrol 2012; 27: 55–63. [PubMed: 21688189]
38. Hopp K, Ward CJ, Hommerding CJ, et al. Functional polycystin-1 dosage governs autosomal dominant polycystic kidney disease severity. J Clin Invest 2012; 122: 4257–4273. [PubMed: 23064367]
39. Takakura A, Nelson EA, Haque N, et al. Pyrimethamine inhibits adult polycystic kidney disease by modulating STAT signaling pathways. Hum Mol Genet 2011; 20: 4143–4154. [PubMed: 21821671]
40. Yamaguchi T, Pelling JC, Ramaswamy NT, et al. cAMP stimulates the in vitro proliferation of renal cyst epithelial cells by activating the extracellular signal-regulated kinase pathway. Kidney Int 2000; 57: 1460–1471. [PubMed: 10760082]
41. Yamaguchi T, Nagao S, Wallace DP, et al. Cyclic AMP activates B-Raf and ERK in cyst epithelial cells from autosomal-dominant polycystic kidneys. Kidney Int 2003; 63: 1983–1994. [PubMed: 12753285]
42. Talbot JJ, Shillingford JM, Vasanth S, et al. Polycystin-1 regulates STAT activity by a dual mechanism. Proc Natl Acad Sci U S A 2011; 108: 7985–7990. [PubMed: 21518865]
43. Yamaguchi T, Wallace DP, Magenheimer BS, et al. Calcium restriction allows cAMP activation of the B-Raf/ERK pathway, switching cells to a cAMP-dependent growth-stimulated phenotype. J Biol Chem 2004; 279: 40419–40430. [PubMed: 15263001]
44. Weimbs T, Talbot JJ. STAT3 Signaling in Polycystic Kidney Disease. Drug Discov Today Dis Mech 2013; 10: e113–e118. [PubMed: 26523147]
45. Talbot JJ, Song X, Wang X, et al. The cleaved cytoplasmic tail of polycystin-1 regulates Srcdependent STAT3 activation. J Am Soc Nephrol 2014; 25: 1737–1748. [PubMed: 24578126]
46. Rowe I, Chiaravalli M, Mannella V, et al. Defective glucose metabolism in polycystic kidney disease identifies a new therapeutic strategy. Nat Med 2013; 19: 488–493. [PubMed: 23524344]
47. Torres JA, Kruger SL, Broderick C, et al. Ketosis Ameliorates Renal Cyst Growth in Polycystic Kidney Disease. Cell metabolism 2019; 30: 1007–1023 e1005. [PubMed: 31631001]
48. Leonhard WN, Song X, Kanhai AA, et al. Salsalate, but not metformin or canagliflozin, slows kidney cyst growth in an adult-onset mouse model of polycystic kidney disease. EBioMedicine 2019; 47: 436–445. [PubMed: 31473186]
49. Flowers EM, Sudderth J, Zacharias L, et al. Lkb1 deficiency confers glutamine dependency in polycystic kidney disease. Nature communications 2018; 9: 814.
50. Hart GW, Slawson C, Ramirez-Correa G, et al. Cross talk between O-GlcNAcylation and phosphorylation: roles in signaling, transcription, and chronic disease. Annu Rev Biochem 2011; 80: 825–858. [PubMed: 21391816]
51. Tan EP, Villar MT, L E, et al. Altering O-linked beta-N-acetylglucosamine cycling disrupts mitochondrial function. J Biol Chem 2014; 289: 14719–14730. [PubMed: 24713701]
52. Tian JL, Qin H. O-GlcNAcylation Regulates Primary Ciliary Length by Promoting Microtubule Disassembly. iScience 2019; 12: 379–391. [PubMed: 30796923]

53. Yu F, Li T, Sui Y, et al. O-GlcNAc transferase regulates centriole behavior and intraflagellar transport to promote ciliogenesis. Protein Cell 2020.
54. Gerakopoulos V, Ngo P, Tsiokas L. Loss of polycystins suppresses deciliation via the activation of the centrosomal integrity pathway. Life Sci Alliance 2020; 3.
55. Upadhyay VS, Muntean BS, Kathem SH, et al. Roles of dopamine receptor on chemosensory and mechanosensory primary cilia in renal epithelial cells. Front Physiol 2014; 5: 72. [PubMed: 24616705]
56. RF R, Fukui H, Chow R, et al. The cilium as a force sensor-myth versus reality. J Cell Sci 2019; 132.
57. Besschetnova TY, Kolpakova-Hart E, Guan Y, et al. Identification of signaling pathways regulating primary cilium length and flow-mediated adaptation. Curr Biol 2010; 20: 182–187. [PubMed: 20096584]
58. Nauli SM, Alenghat FJ, Luo Y, et al. Polycystins 1 and 2 mediate mechanosensation in the primary cilium of kidney cells. Nat Genet 2003; 33: 129–137. [PubMed: 12514735]
59. Praetorius HA, Spring KR. Removal of the MDCK cell primary cilium abolishes flow sensing. J Membr Biol 2003; 191: 69–76. [PubMed: 12532278]
60. Praetorius HA, Frokiaer J, Nielsen S, et al. Bending the primary cilium opens Ca2+-sensitive intermediate-conductance K+ channels in MDCK cells. J Membr Biol 2003; 191: 193–200. [PubMed: 12571753]
61. Liu X, Vien T, Duan J, et al. Polycystin-2 is an essential ion channel subunit in the primary cilium of the renal collecting duct epithelium. eLife 2018; 7.
62. Torres-Perez JV, Naeem H, Thompson CL, et al. Nanoscale Mapping Reveals Functional Differences in Ion Channels Populating the Membrane of Primary Cilia. Cell Physiol Biochem 2020; 54: 15–26. [PubMed: 31916734]
63. Hirano T, Katoh Y, Nakayama K. Intraflagellar transport-A complex mediates ciliary entry and retrograde trafficking of ciliary G protein-coupled receptors. Mol Biol Cell 2017; 28: 429–439. [PubMed: 27932497]
64. Han S, Miyoshi K, Shikada S, et al. TULP3 is required for localization of membrane-associated proteins ARL13B and INPP5E to primary cilia. Biochem Biophys Res Commun 2019; 509: 227–234. [PubMed: 30583862]
65. Wann AK, Knight MM. Primary cilia elongation in response to interleukin-1 mediates the inflammatory response. Cell Mol Life Sci 2012; 69: 2967–2977. [PubMed: 22481441]
66. Fu S, Thompson CL, Ali A, et al. Mechanical loading inhibits cartilage inflammatory signalling via an HDAC6 and IFT-dependent mechanism regulating primary cilia elongation. Osteoarthritis Cartilage 2019; 27: 1064–1074. [PubMed: 30922983]
67. Degrell P, Cseh J, Mohas M, et al. Evidence of O-linked N-acetylglucosamine in diabetic nephropathy. Life Sci 2009; 84: 389–393. [PubMed: 19302818]
68. Gellai R, Hodrea J, Lenart L, et al. Role of O-linked N-acetylglucosamine modification in diabetic nephropathy. American journal of physiology Renal physiology 2016; 311: F1172–F1181. [PubMed: 27029430]
69. Silva-Aguiar RP, Bezerra NCF, Lucena MC, et al. O-GlcNAcylation reduces proximal tubule protein reabsorption and promotes proteinuria in spontaneously hypertensive rats. J Biol Chem 2018; 293: 12749–12758. [PubMed: 29954945]
70. Xu TH, Sheng Z, Li Y, et al. OGT knockdown counteracts high phosphate-induced vascular calcification in chronic kidney disease through autophagy activation by downregulating YAP. Life Sci 2020; 261: 118121. [PubMed: 32693242]
71. Feng D, Sheng-Dong L, Tong W, et al. O-GlcNAcylation of RAF1 increases its stabilization and induces the renal fibrosis. Biochim Biophys Acta Mol Basis Dis 2020; 1866: 165556. [PubMed: 31521821]
72. Hu J, Chen R, Jia P, et al. Augmented O-GlcNAc signaling via glucosamine attenuates oxidative stress and apoptosis following contrast-induced acute kidney injury in rats. Free Radic Biol Med 2017; 103: 121–132. [PubMed: 28017896]
73. Ong Q, Han W, Yang X. O-GlcNAc as an Integrator of Signaling Pathways. Front Endocrinol (Lausanne) 2018; 9: 599. [PubMed: 30464755]

74. Torra R, Badenas C, Darnell A, et al. Linkage, clinical features, and prognosis of autosomal dominant polycystic kidney disease types 1 and 2. J Am Soc Nephrol 1996; 7: 2142–2151. [PubMed: 8915974]

Translational Statement

In ADPKD mouse models, *Ttc21b* deficiency has an attenuating role that is dependent on kidney maturation stage and nephron segment. This suggests cilia function may be influenced by differential factors in the microenvironments of developing versus mature kidneys and between nephron segments, affecting renal cystogenesis and inflammation. Further, O-GlcNAc levels, which may tune metabolism and ciliogenesis in response to the nutrient environment, are increased in kidneys of ADPKD mice, but reduced by *Ttc21b* deficiency in adult ADPKD mice. Thus, elevated O-GlcNAc levels may be a pathological feature of ADPKD and may present potential biomarker and therapeutic opportunities.

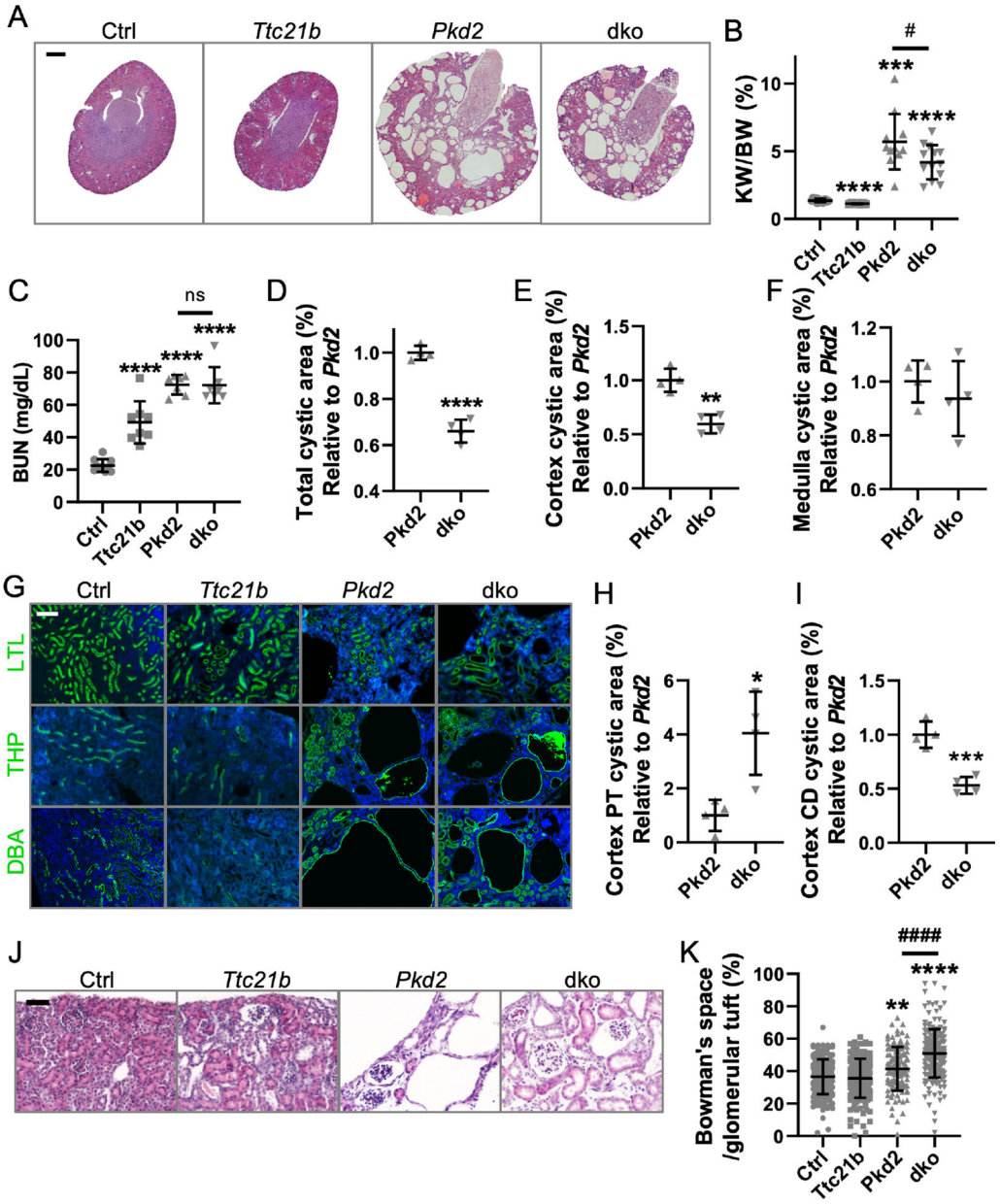

Figure 1. *Ttc21b* deletion in juvenile *Pkd2* conditional knock-out mice reduces cortical cystogenesis.

Representative images of (A) H&E staining of P21 kidney sections. 200X magnification; Scale bar - 500μm. (B) KW/BW ratios (C) BUN levels (D) Percent cystic area of whole kidney; (E) of cortex; (F) and of medulla. *Pkd2* cko values are set at 1. Bars represent mean ± SD. Statistical significance was determined by Brown-Forsythe and Welch ANOVA tests followed by Dunnett's T3 multiple comparisons test in (B), and ordinary one-way ANOVA test followed by Sidak's multiple comparisons test in (C). ***p<0.001, ****p<0.0001, compared to Ctrl. $^{\#\#}$p<0.05, between *Pkd2* cko and dko. In (B) and (C), unpaired t-test was used to determine the difference between *Pkd2* and dko. In (D), (E) and (F), statistical significance was determined by unpaired two-tailed t-test. **p<0.01, ****p<0.0001, compared to Ctrl. Each data point represents a mouse. (G) Staining of

kidney cortices with Lotus Tetragonolobus Lectin (LTL; green), Tamm-Horsfall Protein (THP; green) and Dolichus Biflorus Agglutinin (DBA; green). 100X magnification; Scale bar - 100μm (H) Quantification of LTL+ dilations and (I) DBA+ cystic index in renal cortex. *Pkd2* cko values are set at 1. Bars represent mean ± SD. Statistical significance was determined by unpaired two-tailed t-test. *p<0.05, ***p<0.001, relative to Ctrl. (J) H&E staining. 200X magnification; Scale bar - 50μm (K) Area of Bowman's space/total area of Bowman's capsule. Total area of Bowman's capsule consists of glomerulus and Bowman's space. Bars represent mean ± SD. Statistical significance was determined by Kruskal-Wallis test followed by Dunn's multiple comparisons test. ####p<0.0001, between *Pkd2* cko and dko; **p<0.01 compared to Ctrl; ****p<0.0001 compared to Ctrl

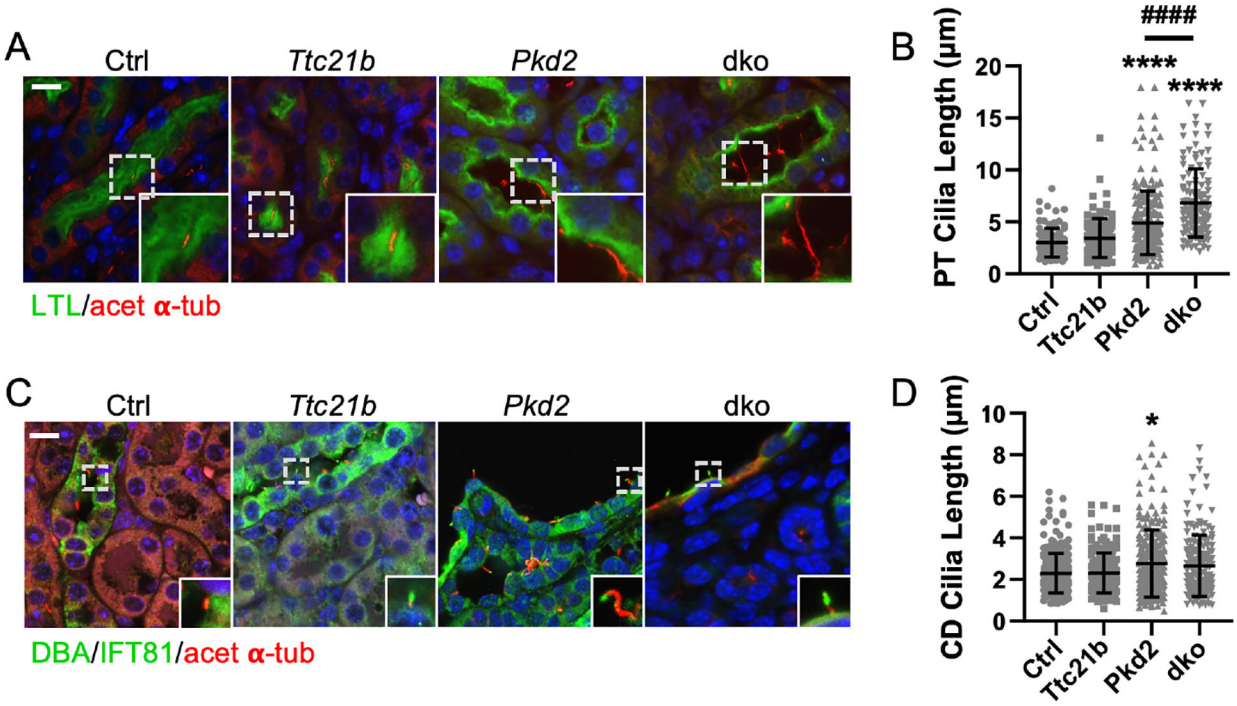

Figure 2. Perinatal *Pkd2* deletion increases renal epithelial primary cilia lengths

(A) Representative images of kidney inner cortices immunostained for acetylated α-tubulin (red) together with LTL (green). Images of the inner cortices were compared across the genotypes to ensure similar nephron segments were assessed. 630X magnification; Scale bar - 10μm. (B) Quantification of cilia length of LTL+ cells. (C) Immunostaining of kidney inner cortices for acetylated α-tubulin (red) and IFT81 (green) together with DBA (green). 630X magnification; Scale bar - 10μm. n=3 mice/genotype. Insets are magnified 3X from original image and show representative cilia. (D) Quantification of cilia length of cortical DBA+ cells. Bars represent mean ± SD. Statistical significance was determined by Kruskal-Wallis test followed by Dunn's multiple comparisons test. *p<0.05, ****p<0.0001, compared to Ctrl; $^{\#\#\#\#}$p<0.0001, between *Pkd2* cko and dko.

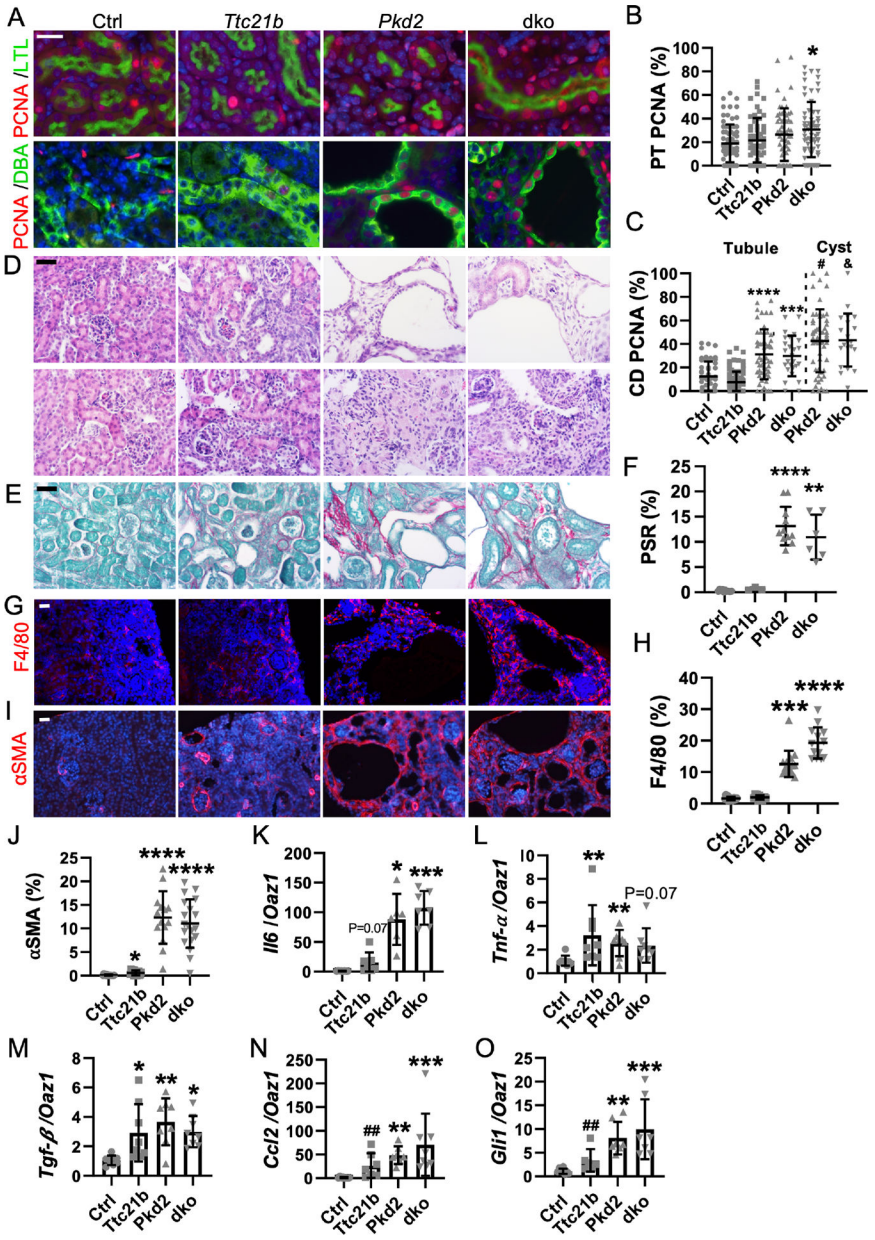

Figure 3. Perinatal *Ttc21b* deletion increases inflammation.

(A) Representative images of kidney cortices immunostained for proliferating cell nuclear antigen (PCNA; red) together with LTL or DBA (green). 400X magnification; Scale bar - 10μm. (B) Percent PCNA+ cells per LTL+ and (C) DBA+ tubule. Each dot represents a tubule or a cyst from n=3 mice/genotype. Bars represent mean ± SD. Statistical significance was determined by Kruskal-Wallis test followed by Dunn's multiple comparisons test. *p<0.05, ***p<0.001, ****p<0.0001, compared to Ctrl. Unpaired t-test was used to determine the difference between non-cystic tubules and cysts. #P<0.05, compared to *Pkd2* cko non-cystic tubule; &P<0.05, compared to dko non-cystic tubule. (D) H&E staining. Upper panels show interstitial space in *Pkd2* cko and dko kidneys. Bottom panels show infiltrating cells. (E) Picrosirius red staining (PSR). 400X magnification; Scale bar - 25μm;

(F) Quantification of PSR. (G) Immunostaining for F4/80 (red) and (H) alpha smooth muscle actin (αSMA; red). 200X magnification; Scale bar - 50μm. Note a few F4/80+ cells and normal αSMA staining around blood vessels in control kidney. (I) Quantification of F4/80 and (J) αSMA staining. Each dot represents percentage of staining of a 200X or 400X magnified image (4–5 images/mouse) from n=3 mice/genotype. (K, L, M, N, O) qPCR. Each dot represents a mouse. In (J) and (K), statistical significance was determined by Brown-Forsythe and Welch ANOVA tests followed by Dunnett's T3 multiple comparisons test. In (K), Unpaired t test with Welch's correction was used to determine the difference between ctrl and *Ttc21b* cko groups. In (F), (I), (L), (N) and (O), statistical significance was determined by Kruskal-Wallis test followed by Dunn's multiple comparisons test. In (N) and (O), Mann Whitney test was used to determine the difference between ctrl and *Ttc21b* cko groups. In (M), statistical significance was determined by ordinary one-way ANOVA followed by Sidak's multiple comparisons test. *$p<0.05$, **$p<0.01$, ***$p<0.001$, ****$p<0.0001$, compared to Ctrl. Bars represent mean ± SD.

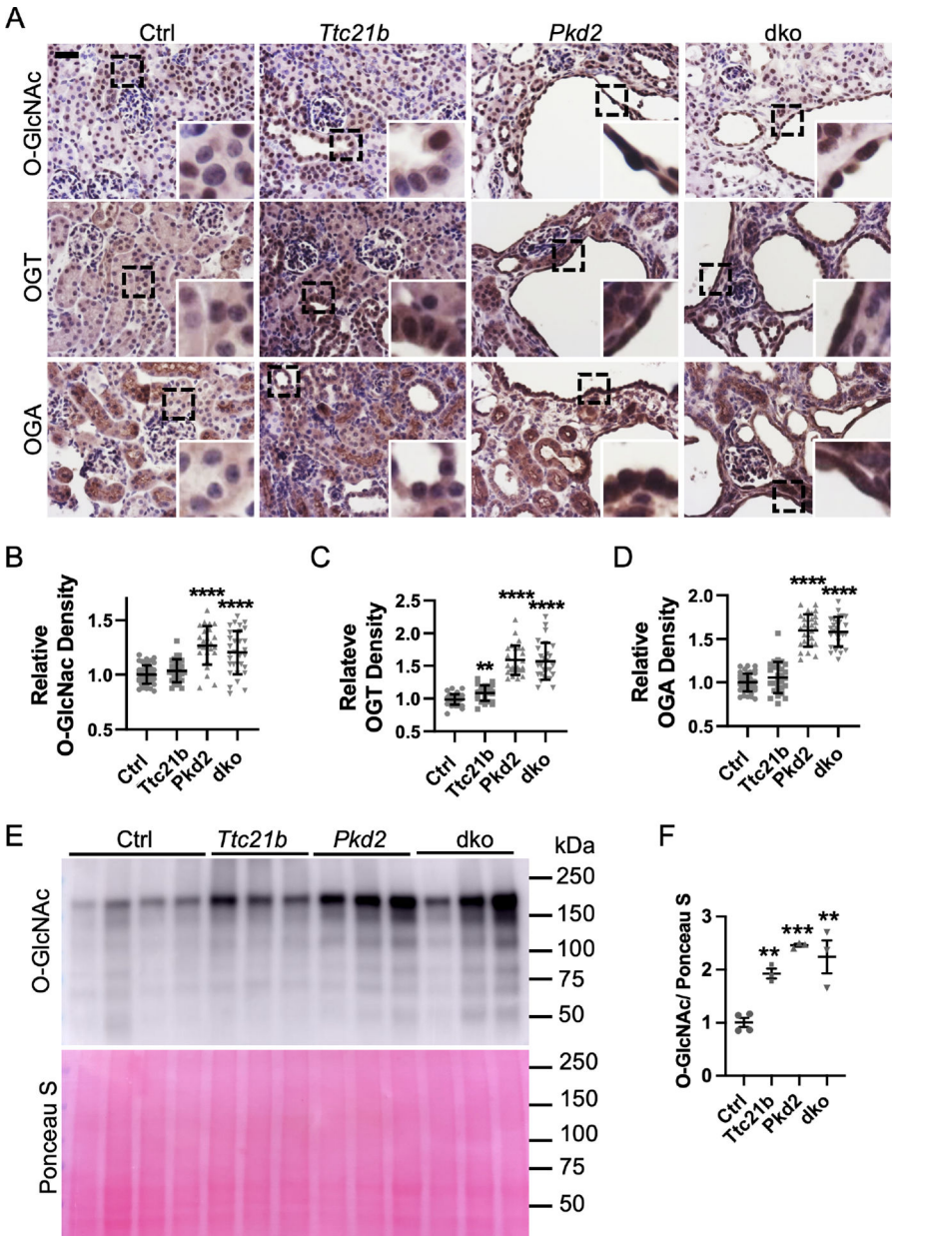

Figure 4. O-GlcNAc is increased in cells lining dilations and cysts in juvenile mice.

(A) Representative images of kidney cortex following immunohistochemistry for O-GlcNAc, OGT and OGA. 400x magnification; Scale bar - 25μm. Insets are magnified 2.5X from original image. n=3 mice/genotype. (B) Quantification of O-GlcNAc; (C) OGT; and (D) OGA IHC. Statistical significance was determined by Brown-Forsythe and Welch ANOVA tests followed by Dunnett's T3 multiple comparisons test. ****p<0.0001, compared to Ctrl. (E) Western blot for O-GlcNAc and (F) Western blot quantification. Images of the Ponceau-stained membranes were converted to 8-bit grayscale images. Whole lanes of the O-GlcNAc Western blots and the Ponceau-stained membranes were selected and six peaks corresponding to bands within each lane were used in the quantifications.

Statistical significance was determined by ordinary one-way ANOVA followed by Tukey's test. **p<0.01, ***p<0.001, compared to Ctrl.

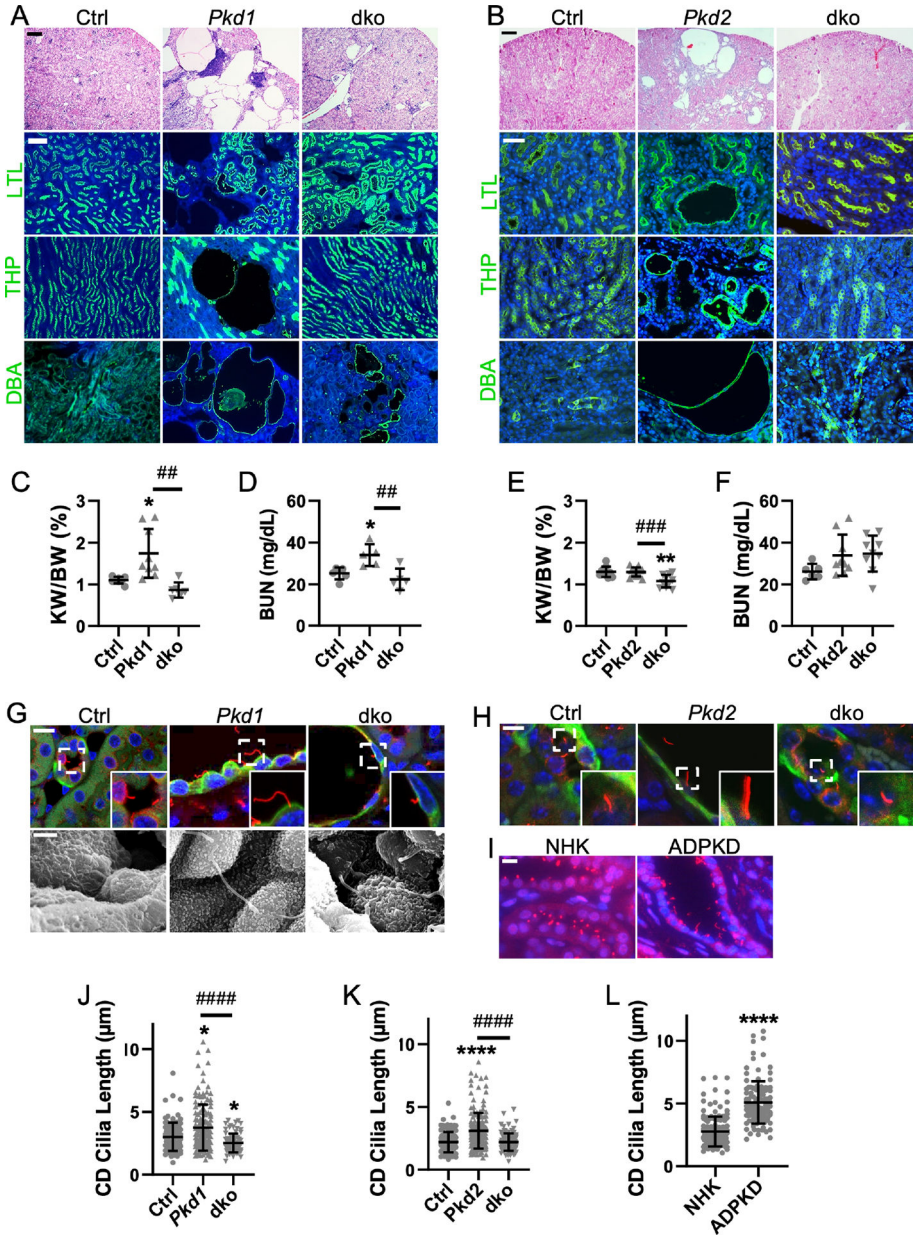

Figure 5. *Ttc21b* deletion in adult ADPKD mouse models attenuates renal cystogenesis and cilia lengthening.

(A) Representative histology, lectin staining and immunostaining (green) for *Pkd1* cko mice and (B) *Pkd2* cko mice. 40X magnification; Scale bars (black) - 250μm. 100X and 200X magnification; Scale bars (white) - 100μm and 50μm in (A) and (B), respectively. (C) KW/BW ratios and (D) BUN levels for *Pkd1* cko and (E, F) *Pkd2* cko mice. Bars represent mean ± SD. Each dot represents an animal. In (C), statistical significance was determined by Brown-Forsythe and Welch ANOVA tests followed by Dunnett's T3 multiple comparisons test. In (D) and (E), statistical significance was determined by one-way ANOVA followed by Tukey's test. In (F), statistical significance was determined by Kruskal-Wallis test followed by Dunn's multiple comparisons test. *p<0.05, **p<0.01, compared to Ctrl; $^{\#\#}$p<0.01; $^{\#\#\#}$p<0.001, between *Pkd1* or *Pkd2* cko and dko. (G) Representative images of *Pkd1* cko

kidney cortex immunostained for acetylated α-tubulin (red) together with DBA (green). 630X magnification; Scale bar - 10μm. Insets are magnified 2X from original image and show representative cilia. Scanning electron micrographs of primary cilia. 10,000X magnification. Scale bar - 1.5μm. n=3 mice/genotype. (H) Images of *Pkd2* cko kidney cortex immunostained for acetylated α-tubulin (red) together with DBA (green). 630X magnification; Scale bar - 10μm. Insets are magnified 2X from original image and show representative cilia. n=3/genotype. (I) Immunostaining for ARL13B (red) of normal human kidney (NHK) and ADPKD renal sections. 630X magnification. Scale bar - 10μm. n=3 for NHK and ADPKD. (J) Quantification of renal cilia lengths of *Pkd1* cko mice, (K) *Pkd2* cko mice, and (L) ADPKD tissue. Cilia lengths were quantified from immunofluorescence experiments of (G, H, I). Significance was determined using Kruskal-Wallis test followed by Dunn's multiple comparisons test (J, K) or by Mann Whitney test (L). Bars represent mean ± SD. $^{\#\#\#\#}p<0.0001$, between *Pkd2* cko and dko; $^{*}p<0.05$, $^{****}p<0.0001$, compared to Ctrl.

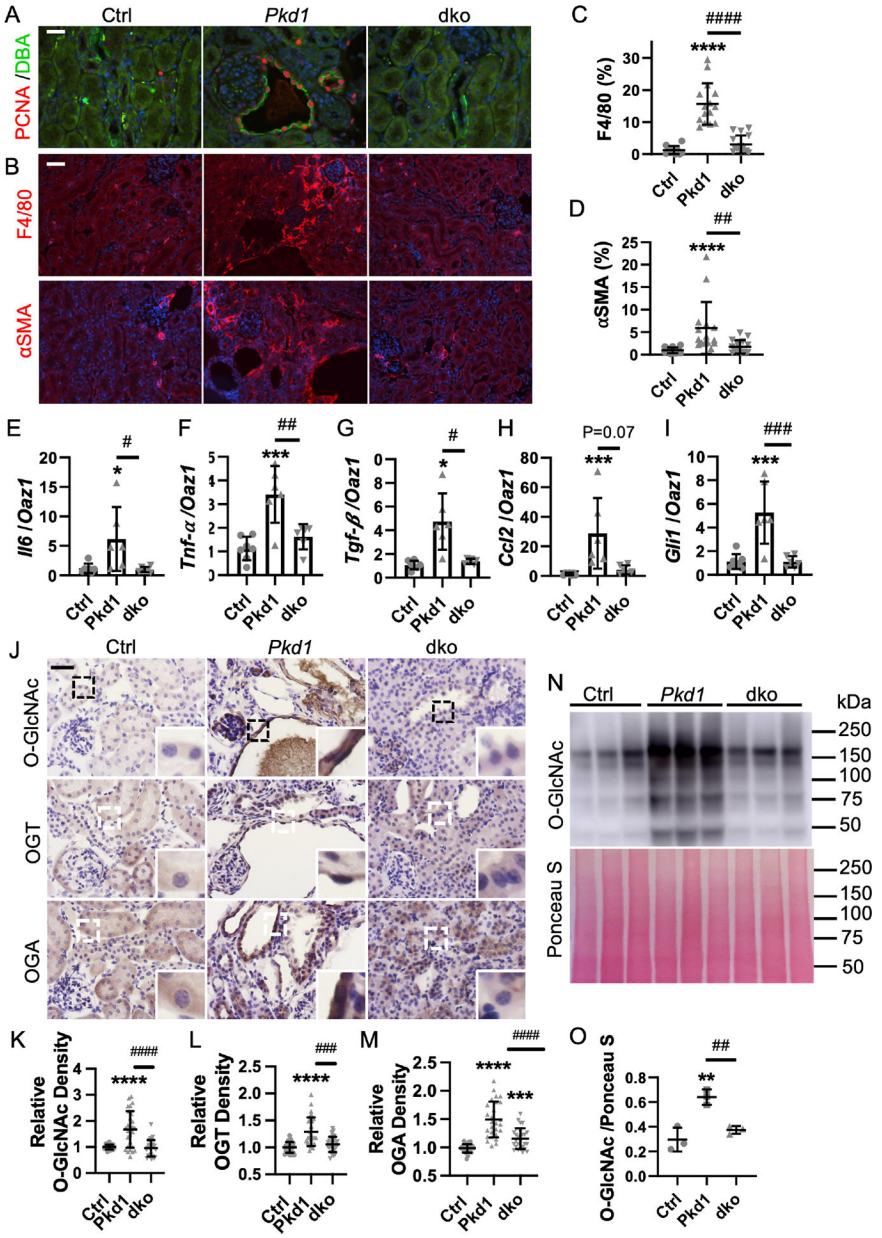

Figure 6. *Ttc21b* deletion in adult *Pkd1* conditional knock-out mice attenuates proliferation, inflammation, increased O-GlcNAc.

(A) Representative images of kidney cortices immunostained for PCNA (red) together with DBA (green). 400X magnification; Scale bar - 25μm. (B) Immunostaining for F4/80 (red) and αSMA (red). 200X magnification; Scale bar - 50μm. (C) Quantification of F4/80 and (D) αSMA staining. Each dot represents percentage of staining of a 200X or 400X magnified image (5 images/mouse) from n=3 mice/genotype. (E, F, G, H, I) qPCR. Each dot represents a mouse. In (C), (D), (E) and (H), statistical significance was determined by Kruskal-Wallis test followed by Dunn's multiple comparisons test. In (F) and (I), statistical significance was determined by ordinary one-way ANOVA test followed by Tukey's multiple comparisons test. In (G), statistical significance was determined by Brown-Forsythe and Welch ANOVA tests followed by Dunnett's T3 multiple comparisons test. *p<0.05,

***p<0.001, compared to Ctrl; #p<0.05, ##p<0.01, ###p<0.001, between *Pkd1* cko and dko. Bars represent mean ± SD. (J) Images of kidney cortices following immunohistochemistry for O-GlcNAc, OGT and OGA. 400X magnification; Scale bar – 20μm. Insets are magnified 4X from the original image and show representative O-GlcNAc, OGT or OGA staining. n=3 mice/genotype. In addition to staining cyst-lining cells, O-GlcNAc was also present in proteinaceous substances within some cysts. (K) Quantification of O-GlcNAc; (L) OGT; and (M) OGA IHC. Statistical significance was determined by Brown-Forsythe and Welch ANOVA tests followed by Dunnett's T3 multiple comparisons test. ****p<0.0001, compared to Ctrl; ###p<0.001, ####p<0.0001, between *Pkd1* cko and dko (N) Western blot for O-GlcNAc (O) Western blot quantification. Statistical significance was determined by ordinary one-way ANOVA test followed by Tukey's multiple comparisons test. **p<0.01, compared to Ctrl. ##p<0.01, between *Pkd1* cko and dko.